Electroreflectance characterization of AlInGaN/GaN high-electron mobility heterostructures

P Yu Bokov , T Brazzini , M F Romero , F Calle , M Feneberg and R Goldhahn

Abstract

Room temperature electroreflectance (ER) spectroscopy has been used to study the fundamental properties of $Al_xIn_yGa_{1-x-y}N$/AlN/GaN heterostructures under different applied bias. The (0001)-oriented heterostructures were grown by metal-organic vapor phase epitaxy on sapphire. The band gap energy of the $Al_xIn_yGa_{1-x-y}N$ layers has been determined from analysis of the ER spectra using Aspnes' model. The obtained values are in good agreement with a nonlinear band gap interpolation equation proposed earlier. Bias-dependent ER allows one to determine the sheet carrier density of the two-dimensional electron gas and the barrier field strength.

Keywords: AlInGaN/GaN, HEMT, electroreflectance

1. Introduction

III-nitride functional devices are based on alloys of the binary end components InN, GaN, and AlN. Whereas in conventional nitride research and technology mostly binary and ternary alloys are discussed, the use of quaternaries in principle opens up a variety of additional possibilities for materials design. For example, the use of quaternary $Al_xIn_yGa_{1-x-y}N$ alloys should allow almost independent control of the lattice parameter and energy band gap by varying the indium and aluminium compositions [1, 2]. This advantage can lead to improvements of the performance of electronic devices as well as to completely new design possibilities beyond what is possible with ternary layers, especially for UV light emitting diodes [3], and radio-frequency high-power transistors [4–7].

For example, one of the main applications of AlInGaN layers is as a barrier of a high electron mobility transistor (HEMT) to replace AlGaN or AlInN. It was shown previously [8] that the insertion of a thin AlN interlayer between the GaN buffer and AlInGaN improved the parameters of such HEMTs significantly, similar to AlInN/GaN HEMTs.

Due to their quaternary nature, AlInGaN semiconducting layers show a broad absorption edge [9]. In fact, it is difficult to determine the absorption edge because of this intrinsic alloy broadening especially at room temperature, and yet there is no fully established method for experimental determination of the AlInGaN band gap energy. Recently, several attempts have been made to determine the fundamental band gap of quaternary nitride alloys. Monroy *et al* grew the quaternaries over a wide compositional range and characterised them by reflectivity and photoluminescence (PL) [10]. Sakalauskas *et al* used spectroscopic ellipsometry to analyze AlInGaN [11].

In this work, electroreflectance (ER) spectroscopy [12–14] was used to investigate the properties of AlInGaN/AlN/GaN heterostructures with different layer composition and

Table 1. Overview of the samples sorted by the thickness of the AlN interlayer. The composition and thickness of the AlInGaN layers is determined by RBS.

Sample	AlN thickness nominal (nm)	AlInGaN thickness (nm)	Al x	In y	Ga $1-x-y$
A	0	13.0	0.618	0.024	0.358
B	0.5	14.0	0.612	0.048	0.340
C	1	12.5	0.594	0.050	0.356
D	2.5	19.0	0.590	0.041	0.368

AlN interlayer thickness at room temperature. In particular, the band gap energies of the quaternary AlInGaN layers have been estimated. By modulation spectroscopic techniques, an electric field within the sample is periodically varied while simultaneously the spectral response is detected. Here, we use ER on nitride heterostructures consisting of a thin quaternary cap layer on top of a GaN buffer, with an AlN spacer layer. The strong electric fields in the quaternary barrier lead to the formation of a two-dimensional electron gas (2DEG) at the AlN/GaN interface. These electric fields can be used for characterization purposes, as shown in this study regarding ER.

2. Samples and experimental details

The four samples under study (see table 1) were designed as HEMT structures and grown on (0001)-oriented sapphire substrates by metal organic vapor phase epitaxy. The samples consist of a 3 μm thick GaN buffer and an AlInGaN barrier with a thickness of around 15 nm. Three of the samples (B, C, and D) additionally have an AlN interlayer between the barrier and the GaN. The compositions and barrier thicknesses, obtained by Rutherford backscattering spectroscopy (RBS), are also shown in table 1.

The samples were processed into simple test devices for ER measurements. We used an ohmic contact (30 nm Ti/200 nm Al/50 nm Ni/150 nm Au) annealed at 850 °C for 30 s in N_2 atmosphere and a semi-transparent Pt Schottky top contact (10 nm). A Pt ring (60 nm) was deposited around the semi-transparent metal layer [8]. Both the ohmic and the ring contacts were bonded to the sample holder for the measurements.

ER determines the relative change in reflectivity ($\Delta R/R$) caused by a change of electric field strength when applying a modulation voltage on the top Schottky contact. Therefore, the light of a Xe-lamp was directed onto the slit of a monochromator with 750 mm focal length and dispersed by a 2400 mm^{-1} grating. The monochromatic light was then focused onto the connected Schottky contact on the sample in quasi-normal incidence. The deviation from normal incidence was <5°. The reflected light intensity was detected by a UV-sensitive Si photodiode as a function of the monochromator wavelength. The absolute value of the generated photocurrent of the Si photodiode corresponds to the reflectivity of the sample under investigation (R) and has been recorded by a digital multimeter, while the signal was additionally preamplified and fed into a lock-in amplifier and the phase-sensitive change of the photocurrent was recorded (ΔR).

The modulation of the reflectivity ΔR is caused by applying a rectangularly modulated voltage to the contacts of the structure [8, 15]. For the quaternary HEMT structures, the voltages were varied between values of +1 and 0, −1,... −11 V, so the amplitude of the modulation voltage ΔU was varied between 0.5 and 6 V. In our case

$$\frac{\Delta R}{R} = \frac{\left(R(U_2) - R(U_1)\right)}{0.5\left(R(U_2) + R(U_1)\right)}, \tag{1}$$

with U_1 and U_2 denoting the two different applied voltages yielding different electric field strengths and thus different reflectivities by change of the dielectric function [16].

The spectral resolution during the ER experiment was better than 1 meV. All measurements were carried out at room temperature. Details of the experimental technique and data analysis of ER can be found elsewhere [12, 13].

3. Experimental results and discussions

3.1. AlInGaN band gap energy

Figure 1 shows a typical ER spectra of our samples. The signals arising from the GaN band gap at around 3.45 eV, the response from the 2DEG, and a further feature in the range of 4.5–4.7 eV are clearly visible. The peaks marked as AlInGaN with arrows in figure 1 are not connected with Franz–Keldysh oscillations originating from the 2DEG and/or the GaN buffer layer, as will be discussed below. Similar results have been obtained in the past with AlGaN/GaN heterostructures [12–14].

To understand the nature of these features, ER spectra under different bias voltages at the Schottky barriers have been recorded. As an example we present ER spectra from sample D at minimum voltages from −10 to 0 V in figure 2. Two spectral features do not change their energy position under voltage variation. At 3.45 eV we identify the signal originating from the GaN buffer layer. The feature at around 4.57 eV is therefore unambiguously related to the quaternary AlInGaN barrier layer. In contrast, the signal connected with the 2DEG (at around 3.55 eV) shifts to lower energies when the minimum voltage is decreased (2DEG depletion). This behavior is typical for all samples under investigation. So, by means of changing the bias we are able to separate different

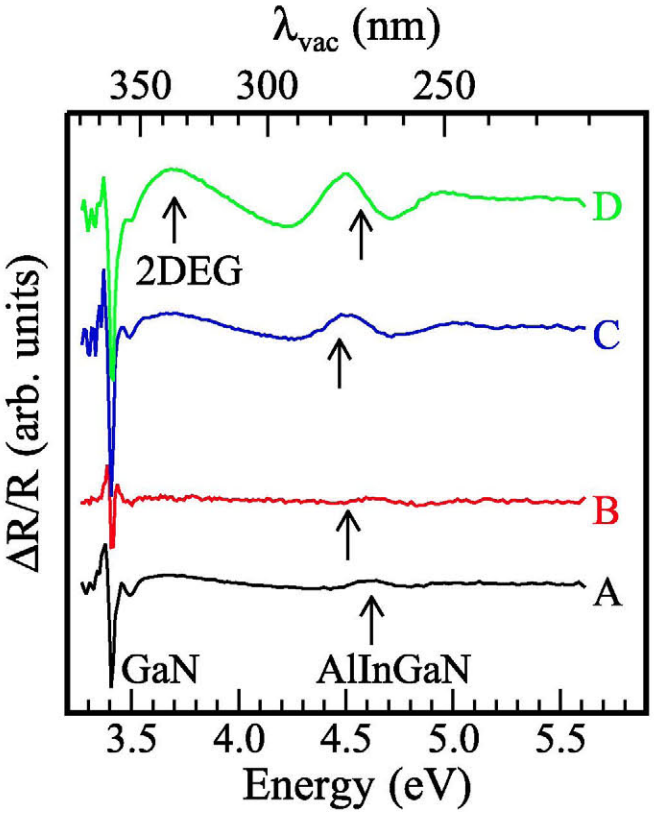

Figure 1. Electroreflectance spectra of the samples under investigation measured at −4 V minimum voltage. The spectra are shifted vertically for better visibility.

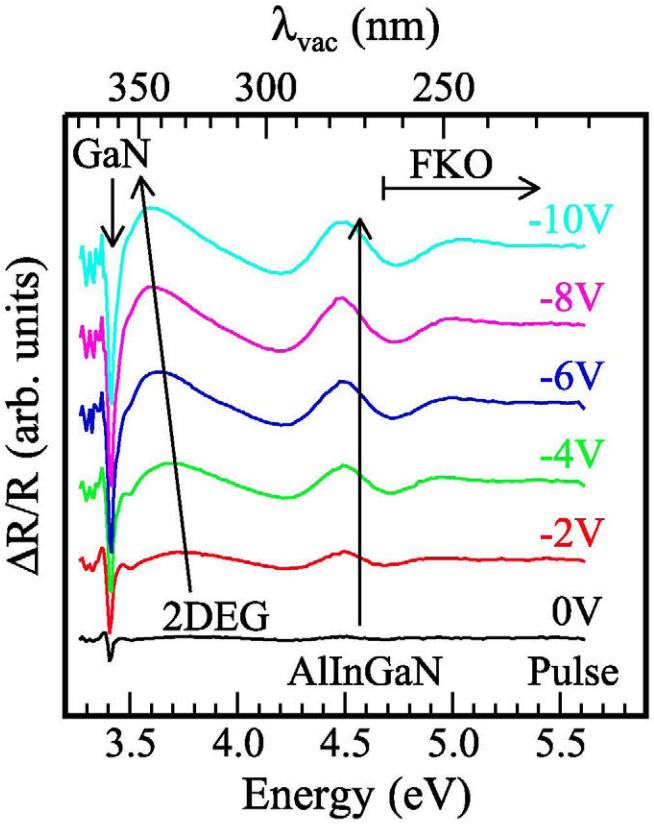

Figure 2. Electroreflectance spectra of sample D measured at different minimum voltages between 0 and −10 V. The spectra are shifted vertically for better visibility. The label FKO marks the region of the Franz–Keldysh oscillations.

signals connected with the band gap related transition in the AlInGaN layer and the 2DEG, respectively.

The energy positions of the features in the ER spectra are directly related to the GaN and AlInGaN band gaps. We determined the band gap values by least-square fits using the model by Aspnes [17]:

$$\frac{\Delta R}{R} = Re\left(\frac{Ae^{i\varphi}}{\left(E - E_g + i\Gamma\right)^m}\right), \tag{2}$$

where A and φ are amplitude and phase parameters, E is the photon energy of the probe beam, E_g is the energy position of the spectral line, Γ is the related broadening parameter, and m is the parameter determining the type of the critical point in Aspnes' original work [17]. We used a value of $m = 2$, which is valid if the transition is of excitonic nature at a M_0 critical point, i.e. the fundamental direct band gap of any nitride semiconductor.

The energy E_g and the Γ parameters are extracted from the fits (shown in figure 3). The fitting parameters are summarized in table 2 and show that the energies of the fundamental transitions in the quaternary layers are in the range of 4.47–4.62 eV. The band gap energy of AlInGaN decreases with increasing In content. These data are fully consistent with the results of [11].

To analyze the experimental data in more detail, we calculated band gap energies for the quaternary layers based on the known RBS compositions. Employing the ternary alloy bowing parameters determined in previous studies, [11] which are based on binary end-point values, we apply the expression [18]:

$$\begin{aligned} E^{\mathrm{AlInGaN}} = {} & (1 - x - y)E^{\mathrm{GaN}} + xE^{\mathrm{AlN}} \\ & + yE^{\mathrm{InN}} - b^{\mathrm{AlGaN}}x(1 - x) \\ & - b^{\mathrm{InGaN}}y(1 - y) + b_{xy}xy, \end{aligned} \tag{3}$$

$$b_{xy} = b^{\mathrm{AlInN}} - b^{\mathrm{AlGaN}} - b^{\mathrm{InGaN}}, \tag{4}$$

where $E^{\mathrm{III-N}}$ are the band gap energies of the allowed transitions for the electric field vector perpendicular to (0001) [19] ($E^{\mathrm{GaN}} = 3.45$ eV, $E^{\mathrm{AlN}} = 6.21$ eV, and $E^{\mathrm{InN}} = 0.68$ eV) and $b^{\mathrm{III-N}}$ are the bowing parameters [19, 20]: $b^{\mathrm{InGaN}} = 1.72$ eV, $b^{\mathrm{AlGaN}} = 0.9$ eV, $b^{\mathrm{AlInN}} = A/(1 + cy^2)$, where $A = 6.43$ eV and $c = 1.21$.

We calculated the band gap energies of the quaternary AlInGaN layers for the case of a fully relaxed crystal and for a fully pseudomorphically strained condition. For the case of pseudomorphic growth on unstrained GaN buffer layers elastic constants [21] and deformation potentials [22] were interpolated linearly. The results of the calculations are summarized in table 2. One can see that the calculated results for the case of relaxed AlInGaN films are in better agreement with the experimental data than those for pseudomorphic growth. The difference between the experimental and calculated band gap energies for fully relaxed AlInGaN diminishes monotonously from 160 meV (for sample A w/o AlN interlayer) to 10 meV (for sample D with the largest thickness of

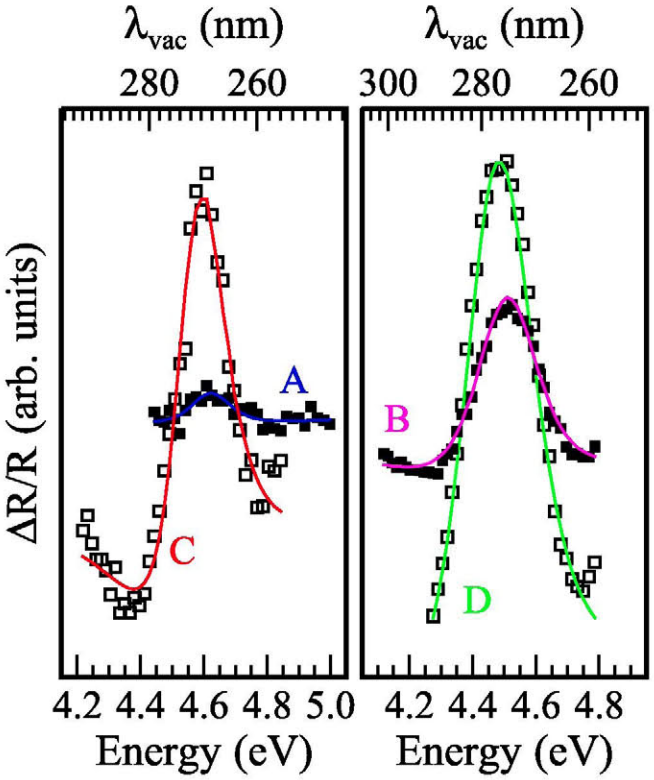

Figure 3. Experimental data (minimum voltage −10 V) connected with the signal from the AlInGaN band gaps (symbols) and the corresponding least-square fits (curves) after equation (2).

Table 2. Band gap energies of the direct allowed transition in the AlInGaN layers with the electric field vector perpendicular to (0001) as determined from fitting Aspnes' model (equation (2)) to ER data compared to the calculated band gap energies for pseudomorphic growth and fully relaxed layers. Additionally, the experimental broadening parameter Γ from Aspnes' model is tabulated. All values are given in eV.

Sample	Experimental Aspnes' model	Calculated (pseudomorphic)	Calculated (relaxed)	Γ
A	4.62	4.48	4.78	0.13
B	4.51	4.36	4.60	0.20
C	4.47	4.28	4.54	0.23
D	4.57	4.34	4.58	0.16

AlN interlayer) with increasing AlN layer thickness. We conclude that inserting the AlN interlayer leads to partial relaxation in the AlInGaN. The broadening parameters of the ER features for the samples are large (0.13–0.23 eV) which we assign to the random alloy broadening in AlInGaN [9]. In figure 4 experimental values for Γ are shown. This parameter increases monotonously with increasing In content. This fact may be connected with the large radius of indium atoms [23] compared to gallium or aluminum atoms.

3.2. 2DEG density

The presence of Franz–Keldysh oscillations in the ER spectra at higher energies than the AlInGaN band gap energy

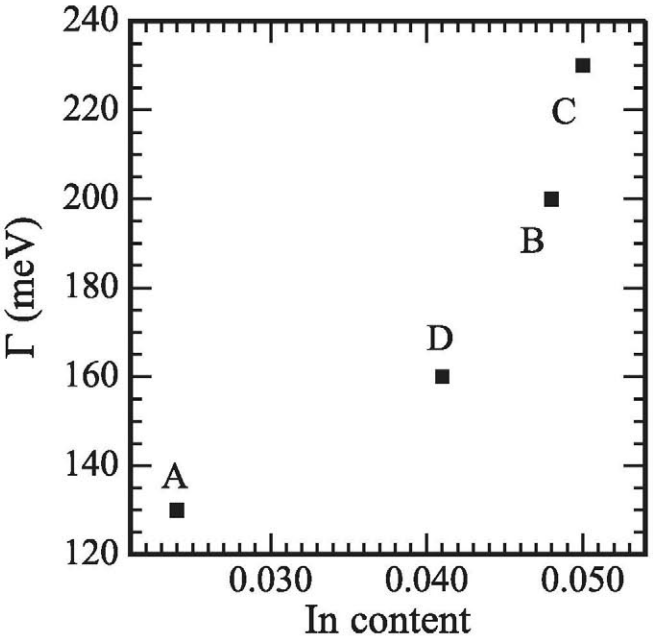

Figure 4. Dependence of the broadening parameter Γ on the indium concentration in the AlInGaN layers.

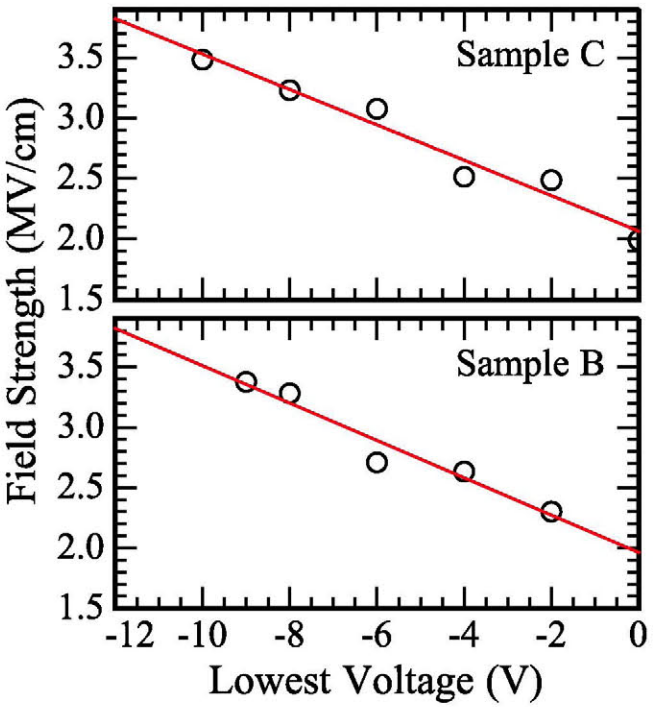

Figure 5. Dependence of the electric field strength in the quaternary barrier layers of samples B and C as a function of the minimum voltage during modulation. Symbols represent measured values extracted from electroreflectance spectra, continuous lines are linear best fits.

(figure 2) yields the possibility of determining the electric field strength in the barrier layer and correspondingly the sheet carrier density in the two-dimensional electron gas [24]. The electro-optical energy $\hbar\Omega$ is obtained by analyzing

Table 3. Lattice parameters and polarisation charge densities of all samples under investigation. The lattice parameters were determined by XRD. The polarisation charges density σ_p^+ on GaN/AlInGaN heterointerface are calculated using the composition data.

Sample	c axis (nm)		σ_p^+
	GaN	AlInGaN	10^{13} (cm^{-2})
A	0.51855	0.5062	2.4
B	0.518	0.5083	1.9
C	0.51855	0.5074	3.3
D	0.51855	0.5056	3.1

Table 4. The 2DEG sheet carrier densities as measured by Hall, *CV*, and ER experiments. N.a. means not available.

Sample	Hall mobility	n_{Hall}	n_{CV}	n_{ER}
	μ (cm^2/Vs)	10^{13} (cm^{-2})	10^{13} (cm^{-2})	10^{13} (cm^{-2})
A	836	3.0	1.77	n.a.
B	899	3.0	n.a.	2.5
C	1070	2.6	1.72	3.1
D	1230	3.4	1.95	3.7

Franz–Keldysh oscillation maxima and minima according to:

$$(\hbar\theta)^{3/2} = \frac{3}{4\pi}\frac{v}{\left(\hbar\omega_v - E_g\right)^{3/2}}, \tag{5}$$

where v is the order of the extremum and $\hbar\omega_v$ the corresponding energy. $\hbar\theta$ is then used to calculate the electric field strength F:

$$F = \frac{\sqrt{2\mu^*}}{\hbar e}(\hbar\theta)^{-3/2}. \tag{6}$$

Here, μ^* is the reduced effective mass and e the elementary charge. The weak ER signal amplitude of AlInGaN layer of sample A does not allow for this analysis, however, the electric field strengths for the other three samples could be obtained. In figure 5 results for samples B and C are given as examples. By linear fitting the electric field strengths as a function of the minimum voltage of the modulation pulses, we estimate the field for zero applied bias. This value is in turn used for determining the sheet carrier density of the 2DEG (n_{ER}) using Gauss's theorem:

$$en_{ER} = \epsilon_0\epsilon_{r,\text{barrier}}F_{\text{barrier}} + \sigma_p^+, \tag{7}$$

where e is the elementary charge, F_{barrier} is the electric field strength in AlInGaN barrier, ϵ_0 is the electric constant, $\epsilon_{r,\text{barrier}}$ is the dielectric constant of the barrier layer which was interpolated according to the composition as determined by RBS, σ_p^+ is the difference of the density of polarization charges, which includes the piezoelectric and spontaneous contributions. These are calculated as the sum of spontaneous and piezoelectric polarization: $\sigma_p^+ = \sigma_{sp} + \sigma_{pz}$, where σ_{sp} is the difference between the interpolated spontaneous polarization parameters and σ_{pz} denotes piezoelectric polarization. σ_{pz} is calculated taking into account the strained situation of the layers with experimental c-lattice parameters given in table 3. These are used along the calculation scheme reported in [25] yielding the values given in table 3. Elastic, piezoelectric and dielectric constants for AlInGaN have been interpolated linearly using data for AlN, GaN, InN [19].

Results and the 2DEG sheet carrier densities as measured by the Hall effect in a van-der-Pauw configuration at 295 K and by capacitance-voltage (*CV*) measurements and by ER are summarized in table 4. The accuracy of the n_{ER} value is connected with the accuracies of F_{barrier} and σ_p^+ and do not exceed in our case 15%. The differences in the determined 2DEG densities obviously stem from different σ_p^+ (see table 3). Additionally, the differences between the sheet carrier densities are connected with the different electric potentials of the Shottky contact during Hall, *CV* and ER measurements. Reasonable agreement is obtained for the results of the 2DEG density measured with the three techniques.

4. Conclusions

In conclusion, ER spectra from AlInGaN/AlN/GaN HEMT-like heterostructures have been recorded at room temperature. The spectral features were separated by applying different bias voltages to a semi-transparent Schottky contact.

The band gap energies of the AlInGaN layers have been determined by least-square fits of the experimental data by Aspnes' model. Modeling of the band gap energy for the quaternary AlInGaN layers shows that the barriers in our structures are partially relaxed. Inserting the AlN interlayer leads to a partial relaxation in the AlInGaN.

The large broadening parameters of the ER lines arise due to the quaternary alloy nature of the films. The values for Γ correlate with the indium concentration in the barrier layers.

Bias dependent ER allows for an independent optical estimation of sheet carrier densities. Sheet carrier densities obtained by ER show reasonable agreement with the results obtained by *CV* and Hall measurements. As a concluding remark, it was shown that ER is a useful method to

characterise the fundamental parameters of quaternary nitride layers.

Acknowledgments

We would like to thank Dr. Jürgen Bläsing, Otto-von-Guericke-Universität Magdeburg, for help with the interpretation of the XRD data. Furthermore, we gratefully acknowledge the supply of samples by AIXTRON AG, Kaiserstr. 98, 52134 Herzogenrath, Germany. This work was financially supported by a DAAD short-term visit grant (Forschungsaufenthalte für Hochschullehrer und Wissenschaftler 2012/2013); by the EU within the 7th RTD Framework (project RAINBOW: Contract No. PITN-GA-2008–213238); by RUE (CSD2009–00046) and CAVE (TEC2012–38247); projects from the Spanish Ministerio de Economía y Competitividad; and by RFBR grants 13–02-01394, 14–02-31510.

References

[1] Lim T, Aidam R, Kirste L, Waltereit P, Quay R, Müller S and Ambacher O 2010 *Appl. Phys. Lett.* **96** 252108
[2] Abid M A, Hassan H Abu, Hassan Z, Ng S S, Bakhori S K Mohd and Raof N H Abd 2011 *Physica* B **406** 1379–84
[3] Muramoto Y, Kimura M and Nouda S 2014 *Semicond. Sci. Technol.* **29** 084004
[4] Lecourt F, Agboton A, Ketteniss N, Behmenburg H, Defrance N, Hoel V, Kalisch H, Vescan A, Heuken M and de Jaeger J-C 2013 *IEEE Electron. Device Lett.* **34** 978
[5] Hahn H, Reuters B, Wille A, Ketteniss N, Benkhelifa F, Ambacher O, Kalisch H and Vescan A 2012 *Semicond. Sci. Technol.* **27** 055004
[6] Kolbe T, Knauer A, Chua C, Yang Z, Kueller V, Einfeldt S, Vogt P, Johnson N M, Weyers M and Kneissl M 2011 *Appl. Phys. Lett.* **99** 261105
[7] Morales F M, Mánuel J M, García R, Reuters B, Kalisch H and Vescan A 2013 *J. Phys. D: Appl. Phys.* **46** 245502
[8] Brazzini T, Pandey S, Romero M F, Yu Bokov P, Feneberg M, Tabares G, Cavallini A, Goldhahn R and Calle F 2013 *Japan. J. Appl. Phys.* **52** 08JK04
[9] Schubert E F, Göbel E O, Horikoshi Y, Ploog K and Queisser H J 1984 *Phys. Rev.* B **30** 813
[10] Monroy E, Gogneau N, Enjalbert F, Fossard F, Jalabert D, Bellet-Amalric E, Si Dang Le and Daudin B 2003 *J. Appl. Phys.* **94** 3121
[11] Sakalauskas E, Reuters B, Khoshroo L R, Kalisch H, Heuken M, Vescan A, Röppischer M, Cobet C, Gobsch G and Goldhahn R 2011 *J. Appl. Phys.* **110** 013102
[12] Goldhahn R, Winzer A T, Dadgar A, Krost A, Weidemann O and Eickhoff M 2007 *Phys. Status Solidi* A **204** 447
[13] Winzer A T, Gobsch G, Goldhahn R, Fuhrmann D, Hangleiter A, Dadgar A and Krost A 2006 *Phys. Rev.* B **74** 125207
[14] Gladysiewicz M, Janicki L, Kudrawiec R, Misiewicz J, Wosko M, Paszkiewicz R, Paszkiewicz B and Tłaczała M 2014 *J. Appl. Phys.* **115** 133504
[15] Avakyants L P, Badgutdinov M L, Yu Bokov P, Chervyakov A V, Shirokov S S, Yunovich A E, Bogdanov A A, Vasil'eva E D, Nikolaev D A and Feopentov A V 2007 *Semiconductors* **41** 1060
[16] Motyka M, Kudrawiec R and Misiewicz J 2007 *Phys. Stat Solidi.* A **204** 354
[17] Aspnes D E 1973 *Surf. Sci.* **37** 418
[18] Wang F, Li S, Xia J, Jiang H X, Lin J Y, Li J and Wei S 2007 *Appl. Phys. Lett.* **91** 061125
[19] Goldhahn R, Buchheim C, Schley P, Winzer A T and Wenzel H 2007 *Nitride Semiconductor Devices: Principles and Simulation* ed J Piprek (Weinheim: Wiley-VCH) p 95
[20] Sakalauskas E, Tuna Ö, Kraus A, Bremers H, Rossow U, Giesen C, Heuken M, Hangleiter A, Gobsch G and Goldhahn R 2012 *Phys. Status Solidi* B **249** 485
[21] Vurgaftman I and Meyer J R 2003 *J. Appl. Phys.* **94** 3675
[22] Wagner G-M and Bechstedt F 2002 *Phys. Status Solidi* B **234** 965
[23] Gorczyca I, Łepkowski S P, Suski T, Christensen N E and Svane A 2009 *Phys. Rev.* B **80** 075202
[24] Winzer A T, Goldhahn R, Gobsch G, Link A, Eickhoff M, Rossow U and Hangleiter A 2005 *Appl. Phys. Lett.* **86** 181912
[25] Feneberg M, Thonke K, Wunderer T, Lipski F and Scholz F 2010 *J. Appl. Phys.* **107** 103517